J Intell Robot Syst (2008) 52:121–138
DOI 10.1007/s10846-008-9207-8

Prosthetic Hand Finger Control Using Fuzzy Sliding Modes

Yunus Ziya Arslan · Yuksel Hacioglu · Nurkan Yagiz

Received: 17 July 2006 / Accepted: 18 January 2008 /
Published online: 20 February 2008

Abstract In order to improve the life quality of amputees, providing approximate manipulation ability of a human hand to that of a prosthetic hand is considered by many researchers. In this study, a biomechanical model of the index finger of the human hand is developed based on the human anatomy. Since the activation of finger bones are carried out by tendons, a tendon configuration of the index finger is introduced and used in the model to imitate the human hand characteristics and functionality. Then, fuzzy sliding mode control where the slope of the sliding surface is tuned by a fuzzy logic unit is proposed and applied to have the finger model to follow a certain trajectory. The trajectory of the finger model, which mimics the motion characteristics of the human hand, is pre-determined from the camera images of a real hand during closing and opening motion. Also, in order to check the robust behaviour of the controller, an unexpected joint friction is induced on the prosthetic finger on its way. Finally, the resultant prosthetic finger motion and the tendon forces produced are given and results are discussed.

Keywords Biomechanical · Index finger · Fuzzy sliding mode control · Tendon force

1 Introduction

To imitate the functionality and motion characteristics of the real human hand, biomimetic studies of the human hand has become important. In several studies, biomechanical models of the human hand fingers have been developed for determining the kinematical and dynamical behaviour of hands and fingers. Armstrong and Chaffin [1] evaluated biomechanical models of interdigit joint-tendon mechanics that have been proposed by Landsmeer [2]. They developed a predictive model of joint and extrinsic finger flexor tendon displacements during pinching and gripping exertions of hands that can be used for

Y. Z. Arslan · Y. Hacioglu (✉) · N. Yagiz
Department of Mechanical Engineering, Faculty of Engineering, Istanbul University,
34320 Avcilar, Istanbul, Turkey
e-mail: yukselh@istanbul.edu.tr

hands and wrists of various sizes. Buchholz and Armstrong [3] aimed to develop a predictive model which is kinematically based and used ellipsoids, for estimating the effects that anthropometry and object size have a prehensile hand posture. Youm et al. [4] carried out an analytical and experimental study to quantitatively determine the kinematic behaviour of the human metacarpophalangeal (MCP) joint which provides the finger mobility and stability required to perform useful task. Buchner et al. [5] presented a kinematic and dynamic model of the human finger in the sagittal plane in order to study finger movements dynamically. They also pointed out the effect of two different optimization algorithms on the muscle forces during finger flexion. An et al. [6], derived a three-dimensional mathematical model of human hand which is based on the quantitative anatomical analysis of 10 fresh cadaver specimens. They used two parameters, "force potential" and "moment potential", for analyzing the constraint of each tendon to the associated joint.

There have been many researches on biomechanical and neuro-physiological properties of muscle systems of the human hand to define the relation between muscular contraction, and variable dynamic movements [7]. The need for the determination of the musculoskeletal forces applied to body segments arises from the desire for improving the life conditions of handicapped people who need prosthetic hand, arm, etc. Prosthetic hands have been designed and developed for about last fifteen years to meet the requirements of the amputated persons [8], [9]. Unfortunately, no prosthetic design has reached the functional features of the human hand, which has magnificent mechanical properties [10]. Today widely used hand prosthesis displays some restrictions on open/grasp movement properties [8]. Besides, many studies on designing artificial hands that more flexible and functional are still under investigation for dexterous applications [11], [12]. There are two main problems to be solved for constructing highly advanced hand prosthetic. The first one is the mechanical design that will allow sufficient freedom of desired movement. The second one is the robust controllers that can handle a more complicated mechanical design.

Movement of the human body is performed by muscles due to applied forces to the skeleton. Function of muscle on skeleton system is force transmission to bones via tendons. In literature, the motion mechanism of the human hand is adopted to robot and prosthetic hand designs to mimic natural movements. Pollard and Gilbert [13] studied to determine the appropriate tendon arrangements of the human hand for optimizing the total muscle force requirements of robot hands. It can be concluded from this study that a robot hand can have a highly similar force capability of the human hand. Li et al. [14] determined the forces produced by extrinsic muscles and intrinsic muscle groups of individual hand fingers by using two 2 dimensional biomechanical models during isometric contractions. Bundhoo and Park [10] designed a biomimetic finger actuated by a type of artificial muscle constituted by Shape Memory Alloys. Weghe et al. [15] constructed an anatomically-correct test bed of the human hand to evaluate its mechanism, function and control. Tsang et al. [16] presented a realistic skeletal musculo-tendon model of the human hand and forearm that this model permits to predict hand and finger position given a set of muscle activations. Fukaya et al. [17] designed a new humanoid-type hand (called TUAT/Karlsruhe Humanoid Hand) with human-like manipulation abilities for adapting to the humanoid robot ARMAR [18].

In last years, many works have been done concerning the tendon driven mechanisms, which consist of belt pulley connections, rotor assembly and serial manipulator. Jacobsen et al. [19] used a derivative and integral controller in order to control a double actuated single joint, which is driven by tendons. Yokoi et al. [20] designed a 7 degrees of freedom (*df*) manipulator which is driven by a coupled tendon mechanism. Also, a joint force control method is formulated that is based on controlling the tendon tension and minimizing the energy consumption in the actuators. Kawanishi et al. [21] designed a tendon driven, 4 *df*

robot finger and used fuzzy logic controller for position control of fingertip. Elasticity of the tendons was also taken into account.

Because of their simplicity, PID controllers are widely used in industrial applications. But, when parameter variations and external disturbances exist, this control method gives poor performance. Thus, it is important to use a robust control method. Due to its robust behaviour, sliding mode control is preferred in robotics and in a variety class of applications. This control method has become widespread after a paper by Utkin [22]. The basic idea of the method is to pull the system states to the sliding surface and then keep the system within a neighbourhood of this surface. A survey paper by Hung et al. [23] gives fundamental theory, main results and practical applications of sliding mode control. Young et al. [24] presented a guide to sliding mode control for practicing control engineers, which offers an accurate assessment of the chattering phenomenon and gives sliding mode design solutions for implementation. Herman [25] proposed a sliding mode controller for a rigid manipulator in terms of the generalized velocity components vector, and this control method was tested on a 3 *df* Yasukawa-like robot. Ertugrul et al. [26] proposed various sliding mode control approaches with different estimation techniques for the equivalent part of the control signal. They used the proposed control techniques to control the two motors of a 6 *df* robotic manipulator. Experimental results have shown that their control method has a good tracking performance. Yagiz [27] discussed the performance of the alternative sliding mode control approaches, where an estimation method for the equivalent control and a chattering elimination method are also included.

In the last decades, some work has been done in order to enhance the performance of the sliding mode controller by integrating it with fuzzy logic algorithms. In general there are two types of fuzzy logic sliding mode controllers. In the first type, fuzzy logic controllers are designed with the sliding mode control principles. It is thought that there exist a sliding line along the diagonal of the rule base, and the control signal has opposite signs at the each side [28]. In the second type, fuzzy logic is used for tuning the parameters of the conventional sliding mode controller, which gives adaptive properties to the controller. Choi and Kim [29] used switching function and its derivative as inputs and discontinuous control gain of sliding mode controller as output. This controller was applied to a robot and successful results were obtained. Tzafestas and Rigatos [30] proposed a new robust fuzzy logic sliding mode controller of the diagonal type, which does not need prior design of the rule base. In this method the control input is decreased or increased according to reaching condition to the sliding surface. Kuo et al. [31] designed a novel controller scheme that the sliding mode and fuzzy sliding mode with an adjustable gain is integrated. For the fuzzy part sliding function is used as input and they have shown that their control method is feasible for the magnetic ball levitation system. Choi et al. [32] proposed a moving switching surface in order to shorten the reaching phase and obtain a system with low sensitivity. In this method switching surface is initially designed to pass the arbitrary initial conditions and subsequently move towards a predetermined switching surface by rotating or/and shifting. Iliev and Kalaykov [33] presented a sliding mode controller for robot manipulators, in which a Takagi-Sugeno fuzzy system is used to describe sliding surface. Each rule of this system represents the maximum slope sliding line for a certain set of parameters given in the premise part. Maximum slope values for the sliding line are obtained by taking into account the variation of the gravity forces acting on the joints of the robot. By simulations, it was shown that transient behaviour is improved.

Since, the prosthetic hand finger will become a part of the human body and, as it is supposed to mimic the natural movements of the human hand, it is important to have more precise and reliable robust controller with high performance. Thus, in this study, a fuzzy

logic sliding mode controller, where the slope of the sliding surface of the conventional sliding mode controller is tuned by a fuzzy logic unit, is used. In this controller, the sliding surface is moved towards the system states in order to construct a sliding motion, faster. Additionally, the robustness of the system is increased, since sliding mode controller is insensitive to parameter variations when the states are on this surface.

2 Anatomy of a Human Hand

Biomechanically, human hand has a very articulated structure and multi-segmented body. Since it has multi degrees of freedom (*df*), it is the highest functional organ of the human body. Human hand has 23 *df* that is provided by 17 joints [34]. If three dimensional movement is taken into consideration, *df* increases to 29 because of orientation and position variation of the hand. In Fig. 1, the joints of a hand are seen.

The phalanges are the small bones that constitute the skeleton of the fingers and thumb. The nearest phalange to the hand body is called "proximal" phalange and the one at the end of the each finger is called "distal" phalange. The distal interphalangeal (DIP) and proximal interphalangeal (PIP) joints have 1 *df* owing to rotational movement and metacarpophalangeal (MCP) joint has 2 *df* owing to adduction–abduction and rotational motions. Except the thumb, the other four fingers (index, middle, ring and little fingers) have similar structure in terms of kinematics and dynamics features. Thumb is the most complex physical structure amongst the hand fingers and different from the fingers in that contains only two phalanges and has 5 *df*. The index finger has the greatest range of motion amongst the fingers such as, for the extension/flexion movement 80^{o} at the DIP joint, 110^{o} at the PIP joint and 90^{o} at the MCP joint. Abduction and adduction angles have been measured as 20^{o} at the MCP joint in the index finger [10].

Muscles show only pulling effect and muscle forces are transmitted to finger bones via tendons. Tendon is a connective tissue that attaches the skeletal muscles to other structures. Tendons are extensions of the muscles in the forearm and the hand. More than fifteen tendons extend from the forearm muscles to hand. While the extension–flexion movement of the hand fingers starts, a set of tendons carries out the extension motion of the finger, and another set of muscles makes the flexion motion (Fig. 2).

Tendon configuration in the hand is complex and this sophisticated tendon arrangement contributes the functionality of human hand motion. Hand extensor tendons, which are on the back side of hand, straighten the fingers and hand flexor tendons on the palm side of hand bend the fingers. In this study, a 3 *df* rigid body chain mechanism is modelled that mimic the size and functionality of the human index finger. Tendon attachment points of the phalanges are reduced in three couples both in the palm side and back side of the hand as

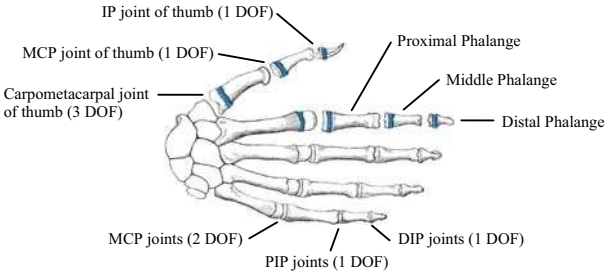

Fig. 1 Skeletal structure of the human hand [35]

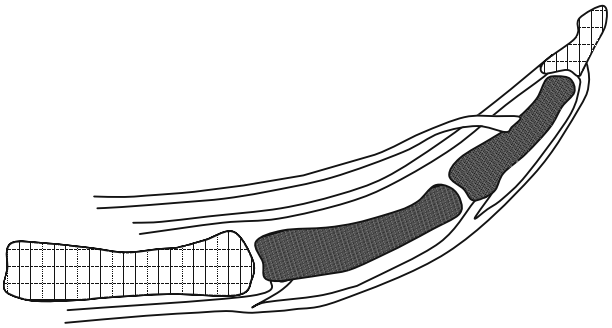

Fig. 2 Flexion and extension tendons of an index finger

seen in Fig. 3. Therefore, the movement of hand flexion is controlled by flexion forces whereas the extension forces are inactive, the opposite is correct for the extension motion.

3 Index Finger Model

Three degrees of freedom prosthetic finger model is used in this study. The proximal, middle and distal phalanges of the index finger of a human hand are modelled similarly to the real index finger in length and mass. Figure 3 gives the physical model of the finger.

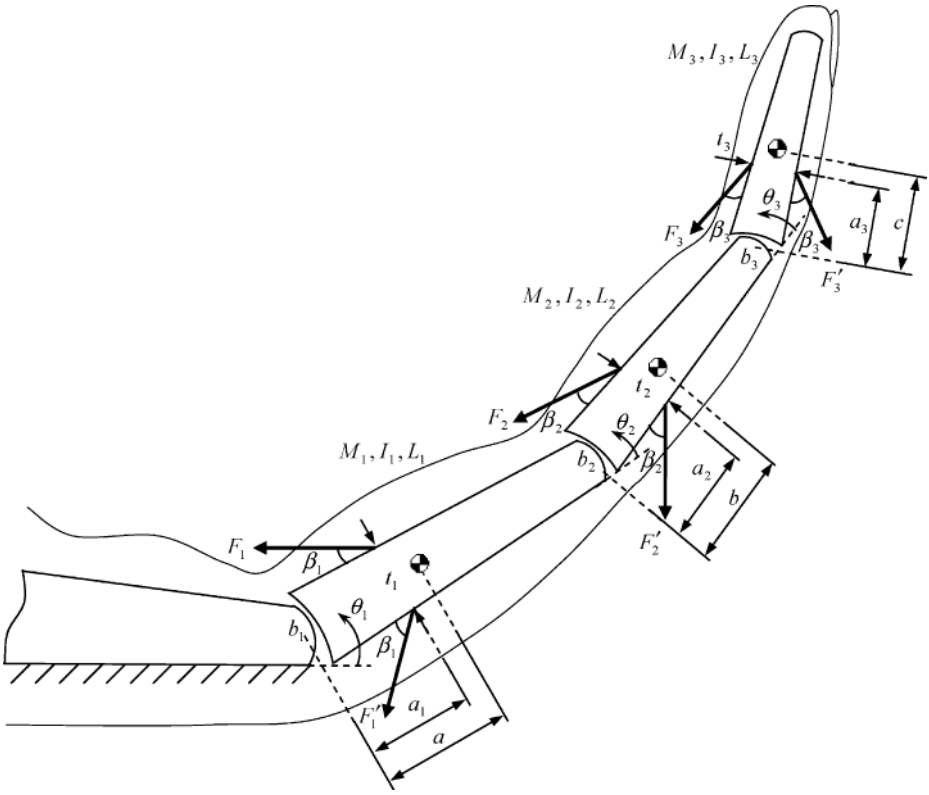

Fig. 3 Prosthetic finger model

F_1, F_2, and F_3 are the flexion forces and F_1', F_2' and F_3' are the extension forces. β_i (i= 1,2,3) is the angle between tendon forces and phalanges. In human hand, the skin tissue covers the finger bones and tendons thus, β_i attains small values and in this study it is 10° each.

M_i, I_i and L_i are the mass, mass moment of inertia and length of the related links. a, b and c are the distances of the mass centre of the first, second and third link, respectively. θ_i is the joint angle of the related link and b_i denotes the viscous friction at the joints. a_i is the distance of the tendon attachment point to the related joint and t_i is the diameter of the related link at this point. Numerical parameters of the finger belonging to this model are given in Appendix 1.

Equations of motion are obtained by using Lagrange equations and are given below.

$$[M(\theta)]\ddot{\theta} + \boldsymbol{C}(\theta,\dot{\theta}) + \boldsymbol{G}(\theta) = \boldsymbol{u} \tag{1}$$

Here, $[M(\theta)]$ is n × n mass matrix of the finger, $\boldsymbol{C}(\theta, \dot{\theta})$ is $n\times1$ vector and includes the coriolis terms, centrifugal terms and undesired joint viscous frictions, $\boldsymbol{G}(\theta)$ is $n\times1$ vector of the gravity terms and $\boldsymbol{u}$ is $n\times1$ generalized torque input vector on phalanges which are produced by tendons, n is the *df*. The matrix and vector terms in Eq. 1 are given in Appendix 1.

The tendon forces are obtained using the relation:

$$\boldsymbol{F}_c = [J]^{-T}\boldsymbol{u} \tag{2}$$

where $[J]^{-T}$ is inverse transpose Jacobian [36]. $\boldsymbol{F}_c$ is the vector having the cartesian components of the tendon forces F_1, F_2, F_3. $\boldsymbol{F}_c$, $[J]^T$, $\boldsymbol{u}$ and tendon forces are given in Appendix 2.

4 Fuzzy Sliding Mode Controller Design

Sliding mode control is a variable structure system and it can be applied to non-linear systems successfully even if there are parameter variations and/or external disturbances. In this control method, control input is changed intentionally according to predefined rules, which drives the system states towards a sliding surface and constrain to stay over this surface. Therefore, there are two parts in the design stage of this controller. The first one is definition of the sliding surface in the state space, and the second one is obtaining the control law in order to construct and maintain such a sliding motion.

The state space form of a non-linear dynamic system can be written as

$$\dot{\phi} = \boldsymbol{f}(\phi) + [B]\boldsymbol{u} \tag{3}$$

where $\phi = \left[\phi_1, \ldots, \phi_n, \phi_{n+1}, \ldots, \phi_{2n}\right]^T$. The second half of the states are the time derivatives of the first half for mechanical systems, respectively. $2n$ is the number of the states. In Eq. 3, $\boldsymbol{f}(\phi)$ is the $2n\times1$ vector of the state equations without the control inputs, $\boldsymbol{u}$ is $n\times1$ generalized torque input vector and $[B]$ is $2n\times n$ matrix that its elements are the

coefficients of the generalized control inputs in the state equations. The sliding surface is defined as follows:

$$S = \{\phi : \sigma(\phi, t) = 0\} \tag{4}$$

For a control system, the sliding surface can be selected as

$$\sigma = [G]\Delta\phi \tag{5}$$

Here

$$\Delta\phi = \phi_r - \phi = [\boldsymbol{e}\ d\boldsymbol{e}/dt]^T \tag{6}$$

is the difference between the reference value and system response. $[G]$ includes the sliding surface slopes:

$$[G] = \begin{bmatrix} \lambda_1 & 0 & 0 & 0 & 0 & 1 & 0 & 0 & 0 & 0 \\ 0 & \ddots & 0 & 0 & 0 & 0 & \ddots & 0 & 0 & 0 \\ 0 & 0 & \lambda_i & 0 & 0 & 0 & 0 & 1 & 0 & 0 \\ 0 & 0 & 0 & \ddots & 0 & 0 & 0 & 0 & \ddots & 0 \\ 0 & 0 & 0 & 0 & \lambda_n & 0 & 0 & 0 & 0 & 1 \end{bmatrix}_{n\times 2n} \tag{7}$$

λ_i is the slope parameter and represents the negative value of the each related sliding surface slope.

$$\sigma_i = \lambda_i \boldsymbol{e}_i + \dot{\boldsymbol{e}}_i \tag{8}$$

Since, sliding mode controllers are insensitive to parameter variations when the system states are on the sliding surface, shortening the reaching time to surface improves the robust behaviour of the controller. To achieve this goal, the slope of the surface is tuned such that, it does not wait for the states to reach it on its course statically but at the same time travels to them dynamically. Thus, in this study, the slope parameter of the sliding surface is not constant but tuned by fuzzy logic unit, which cause the system states to be caught by the sliding surface, faster. Figure 4 demonstrates the general structure of the fuzzy logic sliding mode controller (FLSMC$_\lambda$) with adaptive sliding surface slope.

As depicted in Fig. 5, the triangular membership functions are used for the fuzzification of the inputs, which are error $\boldsymbol{e}$ and derivative of error $\dot{\boldsymbol{e}}$. The output is slope parameter λ, which includes the negative values of the sliding surface slopes. Input membership

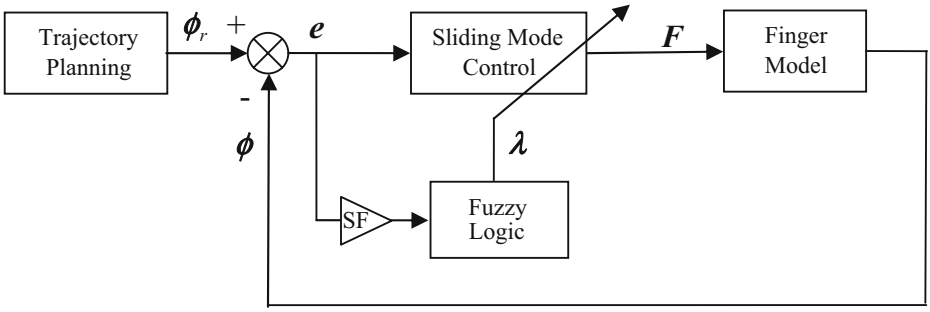

Fig. 4 Fuzzy logic sliding mode controller with adaptive slope (FLSMC$_\lambda$)

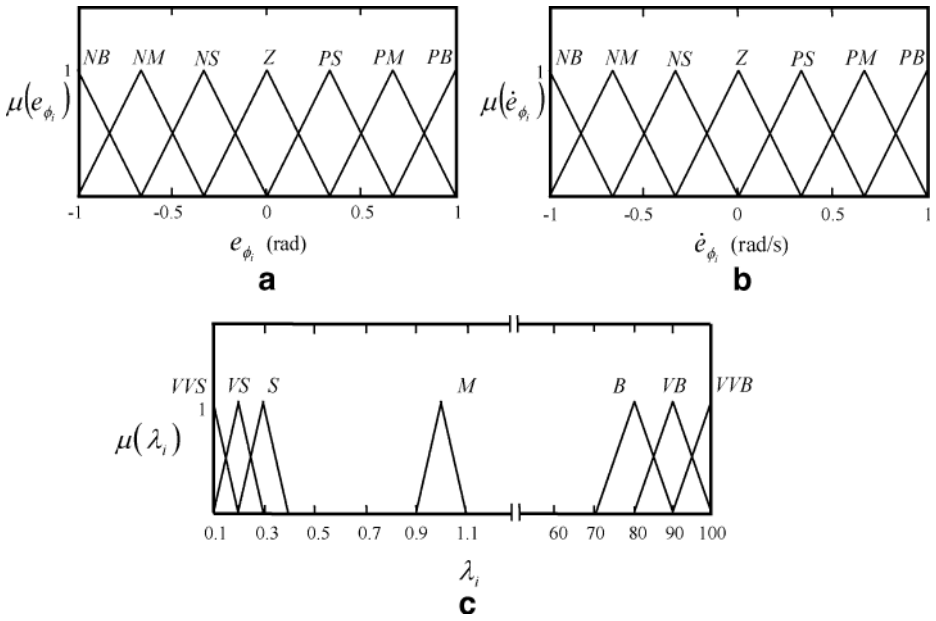

Fig. 5 Membership functions **a** error, **b** derivative of error, **c** slope constant

functions are defined on the [-1,1] closed interval. Thus, in order to map the crisp input variables to their fuzzified values, scaling factors (SF) are used. The scaling factors for the input membership functions and, the range and locations of the output membership functions are found by trial at the design stage. Furthermore, at the design stage, it was concluded that, if all the membership functions overlap each other with 0.5 degree of membership, very small or very big values for the sliding surface slope values could not be attained. Thus, in order to be able to make surface slope value smaller or bigger whenever necessary, for output, membership function *M* is defined around the vicinity of the sliding surface slope value of the classical sliding mode controller and it is separate from the other membership functions.

If the differential Eq. 8 of the sliding surface is solved, it can be seen that, in order to have a stable motion on the sliding surface, each λ_i must be positive. This implies that the sliding surface can only move through the second and fourth quadrants of the $e_{\phi_i} - \dot{e}_{\phi_i}$ phase plane. Thus, the stability of the system when the states are on the sliding surface is

Table 1 Rule table for the slope parameter λ_i

$\dot{e}_{\phi_i}$ / $e_{\phi i}$	NB	NM	NS	*Z*	PS	PM	PB
NB	*M*	*S*	VS	VVS	VS	*S*	*M*
NM	*B*	*M*	*S*	VS	*S*	*M*	*B*
NS	VB	*B*	*M*	*S*	*M*	*B*	VB
Z	VVB	VB	*B*	*M*	*B*	VB	VVB
PS	VB	*B*	*M*	*S*	*M*	*B*	VB
PM	*B*	*M*	*S*	VS	*S*	*M*	*B*
PB	*M*	*S*	VS	VVS	VS	*S*	*M*

preserved as long as the sliding surface moves through the stable regions of the phase plane. The rule table for λ_i is in Table 1. The logic behind this rule table is to move the sliding surfaces towards the error states, resulting in following the desired trajectory more successfully and precisely than the conventional approaches.

As described previously, after defining the sliding surface and fuzzy adjusting of its slope, the control law is to be obtained for constructing the sliding motion. Since the classical sliding mode control method results in chattering because of its Lyapunov function using sign(σ) term, in this study the following Lyapunov function candidate, which is proposed for a non-chattering action is introduced. It has to be positive definite and its derivative has to be negative semi-definite for overall stability [27].

$$\boldsymbol{v}(\sigma) = \frac{\sigma^T \sigma}{2} > 0 \tag{9}$$

$$\frac{\mathrm{d}\boldsymbol{v}(\sigma)}{\mathrm{d}t} = \frac{\dot{\sigma}^T \sigma}{2} + \frac{\sigma^T \dot{\sigma}}{2} \leq 0 \tag{10}$$

If the limit condition is applied to Eq. 10, then

$$\frac{d\,\sigma}{dt} = \frac{d\mathbf{A}(t)}{dt} - [G]\frac{d\,\phi}{dt} = 0 \tag{11}$$

where

$$\boldsymbol{A}(t) = [G]\phi_r \tag{12}$$

From Eqs. 3 and 5

$$\frac{\mathrm{d}\boldsymbol{A}(t)}{\mathrm{d}t} - [G]\big(f(\phi) + [B]\boldsymbol{u}_{\mathrm{eq}}\big) = 0 \tag{13}$$

$\boldsymbol{u}_{\mathrm{eq}}$ is the equivalent control torque input vector for the limit case. Finally equivalent control is found as below,

$$\boldsymbol{u}_{\mathrm{eq}}(t) = [GB]^{-1}\left(\frac{\mathrm{d}\boldsymbol{A}(t)}{\mathrm{d}t} - [G]\boldsymbol{f}(\phi)\right) \tag{14}$$

Equivalent control is valid only on sliding surface. Thus, an additional term should be defined to pull the system to the surface. For this purpose, the derivative of the Lyapunov function can be selected as follows.

$$\dot{\boldsymbol{v}} = -\sigma^T[\Gamma]\sigma < 0 \tag{15}$$

By equating Eqs. 10 to 15 and carrying out necessary manipulations, total control input is found as

$$\boldsymbol{u}(t) = \boldsymbol{u}_{\mathrm{eq}}(t) + [GB]^{-1}[\Gamma]\sigma \tag{16}$$

$[GB]^{-1}$ is always invertible and equal to mass matrix for mechanical systems. [Γ] is a positive definite matrix, and value of terms are decided by trial at the design stage. However, if the knowledge of $\boldsymbol{f}(\phi)$ and [B] are not well known, the equivalent calculated control inputs will be completely different from the actual equivalent control inputs. Thus, in this study, it is

assumed that the equivalent control is the average of the total control [26]. For estimation of the equivalent control, an averaging filter, here a low pass filter, can be designed as follows.

$$T\dot{\hat{\boldsymbol{u}}}_{\mathrm{eq}}(t)+\hat{\boldsymbol{u}}_{\mathrm{eq}}(t)=\boldsymbol{u}(t-\delta t) \tag{17}$$

or in the s-domain

$$\hat{\boldsymbol{u}}_{\mathrm{eq}}(s)=\frac{1}{Ts+1}e^{-(\delta t)s}\boldsymbol{u}(s) \tag{18}$$

δt is the difference between the sampling time. The main idea, which is used in the design stage of the low pass filter, is based on that low frequencies determine the characteristics of the signal and high frequencies come from unmodeled dynamics. It should be noted that, since the proposed fuzzy algorithm moves the sliding surface towards the system states, resulting in a shorter reaching phase, using an averaging filter for the estimation of the equivalent control is feasible. On the other hand, using such estimation minimizes the need for system information for the control input calculation. Finally the non-chattering control input results in,

$$\boldsymbol{u}(t)=\hat{\boldsymbol{u}}_{\mathrm{eq}}(t)+[GB]^{-1}[\Gamma]\sigma \tag{19}$$

5 Trajectory Planning

Trajectory planning is an important stage in the kinematic analysis of prosthetic finger model since it is supposed to mimic the natural movements of the human finger. In this study, the flexion and extension movement of the index finger of a human hand is investigated. Thus, the movement of human hand while fingers are closing and opening was recorded by using a digital camera. During the closing-opening motion of the hand, flexion motion is carried out in 1.92 s and extension motion is carried out from this time to 3.68th second. Then, recorded video was split into frames with 0.08 s time intervals and some of them are given in Fig. 6. Afterwards, these frames were transferred into a computer aided design program where the joint angles were measured with the aid of the marks which are placed on the finger joints at the beginning.

In order to have continuous reference paths for the joint angles, sixth order polynomials were fitted to the experimental data. The experimental data and their polynomial approximations are given in Fig. 7. By using the polynomials as reference, the motion of the end of the distal link is obtained as given in Fig. 7d. The obtained polynomials will be

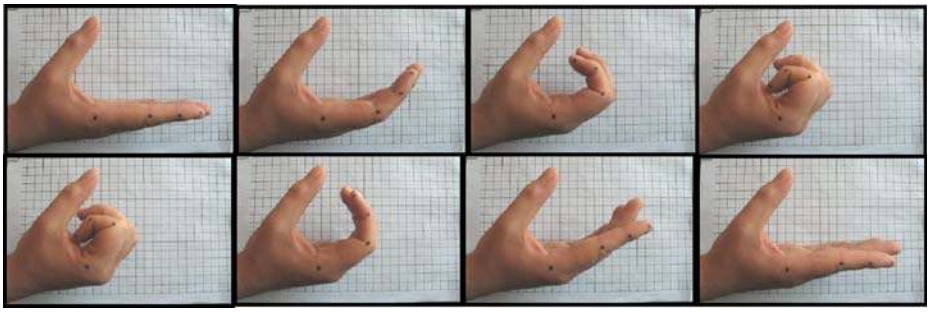

Fig. 6 Some of the camera images of the closing–opening motion of the hand

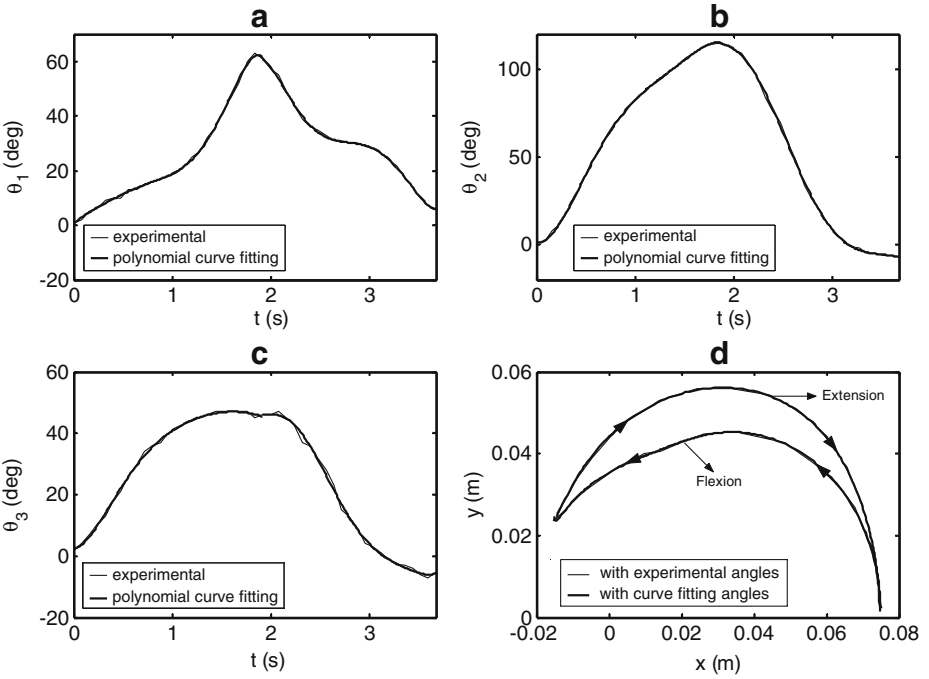

Fig. 7 Experimental and approximated reference values for **a** proximal phalange, **b** middle phalange, **c** distal phalange, **d** reference trajectory of the finger tip with the experimental and approximated values

used as reference joint motions for the fuzzy sliding mode controller through the numerical analysis of the finger model.

6 Results and Discussion

In order to test the robust behaviour of the controller, an unexpected non-linear joint friction fault at PIP joint occurs:

$$T_r = \mu \operatorname{sign}(\dot{\theta}_2) \tag{20}$$

This friction occurs at first second and increases up to its final value 0.001 [Nm], as shown in Fig. 8. Numerical parameters of the controller are given in Appendix 3.

The reference angles and differences between the reference and actual values of the related links are given in Fig. 9. It is clear from this figure that the each joint of the finger tracks the certain trajectory successfully in spite of the unexpected resistive torque, which indicates the efficiency and robustness of the fuzzy sliding mode controller. It is deduced from Fig. 9b that the maximum magnitudes for the error values of the finger joints are below 0.4°.

In Fig. 10, the reference and resultant trajectories of the finger tip are presented.

In Fig. 11, the tendon forces are given. Generalized torques are the output signals of the controller and tendon forces, which are used to manipulate the finger, are obtained from these torques as described in Section 3. At the first second, an unexpected non-linear joint friction is included. Throughout the motion of the finger, flexor tendons are active in the closing

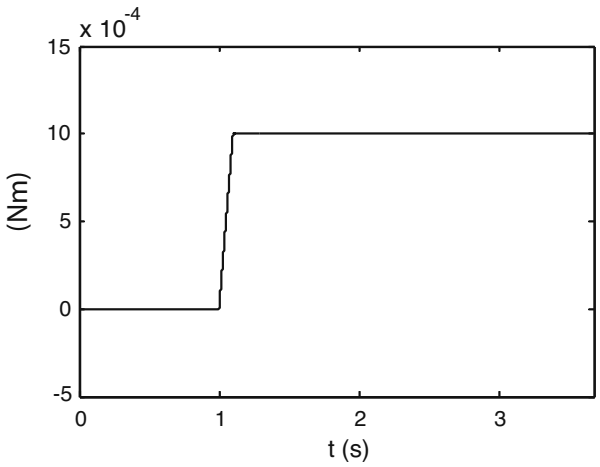

Fig. 8 Applied dry friction to PIP joint

motion and extensor tendons are active in the opening motion. Thus, after 1.92nd second, extension tendon forces are used instead of flexion tendon forces. From the results, it is seen that, maximum tendon forces are obtained for the tendon which actuates proximal phalange and the minimum force average was obtained for the tendon of distal phalange as expected.

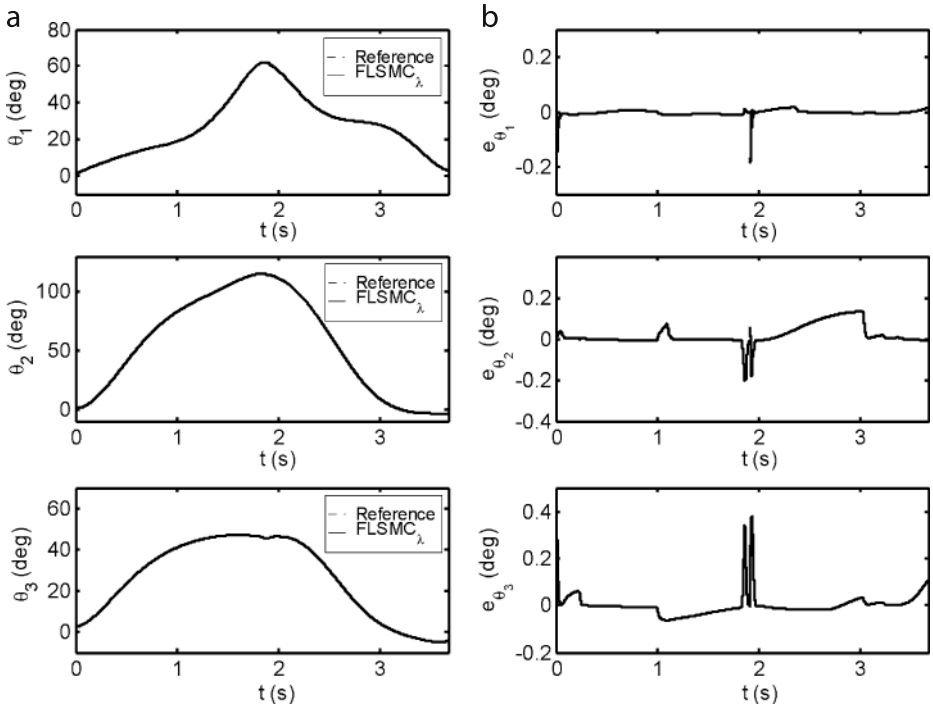

Fig. 9 **a** Reference and actual angle values for the links, **b** Tracking errors for the links

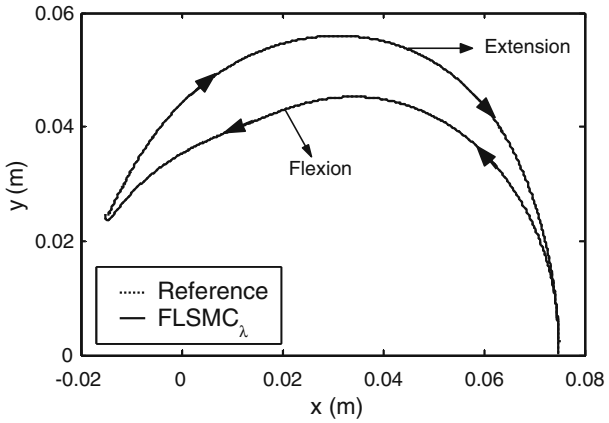

Fig. 10 The reference and resultant trajectories of the finger tip

7 Conclusion

A robust fuzzy sliding mode control of a prosthetic index finger model was proposed in this study which has 3 *df*. The proximal, middle and distal phalanges of the index finger of human hand are modelled similarly to the real index finger in length and mass. The phalanges are actuated by flexor and extensor tendons during the flexion and extension movement of the finger, respectively. Fuzzy sliding mode controller, where the slope constant of sliding mode controller is dynamically updated by a fuzzy logic unit, was used in order to produce the necessary tendon

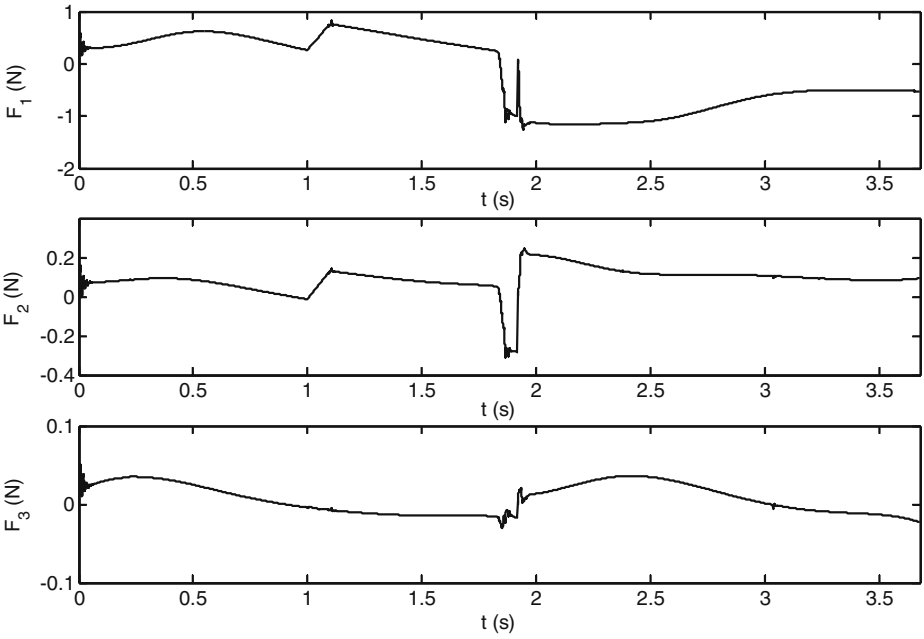

Fig. 11 Tendon forces

forces during the movement of the finger. This control method was preferred due to its robust behaviour and efficient tracking performance. In fact, the numerical results verify that the finger follows its trajectory successfully even in the existence of a non-linear unexpected change in one of the joints and a sudden change in the direction of the finger motion.

Acknowledgement This work is supported by the Research Fund of Istanbul University, Project Number UDP-701/14032007.

Appendix 1

The mass matrix, coriolis-centrifugal vector and gravity vector of the motion equations:

$$[M(\theta)]=\begin{bmatrix} A_1+A_2+A_3+2L_1A_4c_2+2cM_3(L_1c_{23}+L_2c_3) & A_2+A_3+L_1A_4c_2+cM_3(L_1c_{23}+2L_2c_3) & A_3+cM_3(L_1c_{23}+L_2c_3) \\ A_2+A_3+L_1A_4c_2+cM_3(L_1c_{23}+2L_2c_3) & A_2+A_3+2cM_3L_2c_3 & A_3+cM_3L_2c_3 \\ A_3+cM_3(L_1c_{23}+L_2c_3) & A_3+cM_3L_2c_3 & A_3 \end{bmatrix}$$

$$\boldsymbol{C}(\theta,\dot{\theta})=\begin{bmatrix} b_1\dot{\theta}_1-L_1(A_4s_2+cM_3s_{23})\left(2\dot{\theta}_1\dot{\theta}_2+\dot{\theta}_2^2\right)-cM_3(L_1s_{23}+L_2s_3)\left(2\dot{\theta}_1\dot{\theta}_3+2\dot{\theta}_2\dot{\theta}_3+\dot{\theta}_3^2\right) \\ b_2\dot{\theta}_2+\mu\,\mathrm{sign}(\dot{\theta}_2)+L_1(A_4s_2+cM_3s_{23})\dot{\theta}_1^2-cM_3L_2s_3\left(2\dot{\theta}_1\dot{\theta}_3+2\dot{\theta}_2\dot{\theta}_3+\dot{\theta}_3^2\right) \\ b_3\dot{\theta}_3+cM_3\left((L_1s_{23}+L_2s_3)\dot{\theta}_1^2+L_2s_3\left(2\dot{\theta}_1\dot{\theta}_2+\dot{\theta}_2^2\right)\right) \end{bmatrix}$$

$$\boldsymbol{G}(\theta)=\begin{bmatrix} g(A_5c_1+A_6c_{12}+cM_3c_{123}) \\ g(A_6c_{12}+cM_3c_{123}) \\ gcM_3c_{123} \end{bmatrix}$$

where

$$\begin{aligned} A_1 &= M_1a^2+I_1+(M_2+M_3)L_1^2 \\ A_2 &= M_2b^2+I_2+M_3L_2^2 \\ A_3 &= M_3c^2+I_3 \\ A_4 &= M_2b+M_3L_2 \\ A_5 &= M_1a+(M_2+M_3)L_1 \\ A_6 &= M_2b+M_3L_2 \end{aligned}$$

In the expressions above, the abbreviations $c_1=\cos\theta_1$, $s_2=\sin\theta_2$, $c_{123}=\cos(\theta_1+\theta_2+\theta_3)$, $s_{23}=\sin(\theta_2+\theta_3)$ are used.

The numerical parameters are given below:

Parameter	Numerical value	Unit	Parameter	Numerical value	Unit
M_1	0.0090	[kg]	b	0.0091	[m]
M_2	0.0032	[kg]	c	0.0068	[m]
M_3	0.0010	[kg]	a_1	0.0095	[m]
I_1	1.1291×10^{-6}	[kg]	a_2	0.0038	[m]
I_2	1.3303×10^{-7}	[kg]	a_3	0.0027	[m]
I_3	2.3656×10^{-8}	[kg]	t_1	0.0138	[m]
L_1	0.038	[kgm^2]	t_2	0.0113	[m]
L_2	0.021	[kgm^2]	t_3	0.0075	[m]
L_3	0.016	[kgm^2]	β_i	10	[deg]
a	0.0165	[m]	b_i	0.0001	[Nms]

Appendix 2

$[J]^{\mathrm{T}}$, $\boldsymbol{F}_{\mathrm{c}}$ and $\boldsymbol{u}$ are given below.

$$[J]^T = \begin{bmatrix} \frac{\partial x_1}{\partial \theta_1} & \frac{\partial y_1}{\partial \theta_1} & \frac{\partial x_2}{\partial \theta_1} & \frac{\partial y_2}{\partial \theta_1} & \frac{\partial x_3}{\partial \theta_1} & \frac{\partial y_3}{\partial \theta_1} \\ \frac{\partial x_1}{\partial \theta_2} & \frac{\partial y_1}{\partial \theta_2} & \frac{\partial x_2}{\partial \theta_2} & \frac{\partial y_2}{\partial \theta_2} & \frac{\partial x_3}{\partial \theta_2} & \frac{\partial y_3}{\partial \theta_2} \\ \frac{\partial x_1}{\partial \theta_3} & \frac{\partial y_1}{\partial \theta_3} & \frac{\partial x_2}{\partial \theta_3} & \frac{\partial y_2}{\partial \theta_3} & \frac{\partial x_3}{\partial \theta_3} & \frac{\partial y_3}{\partial \theta_3} \end{bmatrix}$$

$$\boldsymbol{F}_c = [F_{1x} \quad F_{1y} \quad F_{2x} \quad F_{2y} \quad F_{3x} \quad F_{3y}]^T \text{ and } \boldsymbol{u} = [u_1 \quad u_2 \quad u_3]^T$$

where

$$x_1 = a_1 \cos\theta_1 - \frac{t_1}{2}\sin\theta_1$$
$$y_1 = a_1 \sin\theta_1 + \frac{t_1}{2}\cos\theta_1$$
$$x_2 = L_1 \cos\theta_1 + a_2 \cos\theta_{12} - \frac{t_2}{2}\sin\theta_{12}$$
$$y_2 = L_1 \sin\theta_1 + a_2 \sin\theta_{12} + \frac{t_2}{2}\cos\theta_{12}$$
$$x_3 = L_1 \cos\theta_1 + L_2 \cos\theta_{12} + a_3 \cos\theta_{123} - \frac{t_3}{2}\sin\theta_{123}$$
$$y_3 = L_1 \sin\theta_1 + L_2 \sin\theta_{12} + a_3 \sin\theta_{123} + \frac{t_3}{2}\cos\theta_{123}$$

Here x_i and y_i (I=1,2,3) denote position of the flexor tendon attachment points of the related phalanges where $\theta_{12}=\theta_1+\theta_2$, $\theta_{123}=\theta_1+\theta_2+\theta_3$.

$$F_{1x} = F_1 \cos\alpha_1; \quad F_{2x} = F_2 \cos\alpha_2; \quad F_{3x} = F_3 \cos\alpha_3$$
$$F_{1y} = F_1 \sin\alpha_1; \quad F_{2y} = F_2 \sin\alpha_2; \quad F_{3y} = F_3 \sin\alpha_3$$

α_i (i=1,2,3) are the angles of the flexor tendon forces with respect to the base frame and are given below.

$$\alpha_1 = \theta_1 + (\pi - \beta_1)$$
$$\alpha_2 = \theta_1 + \theta_2 + (\pi - \beta_2)$$
$$\alpha_3 = \theta_1 + \theta_2 + \theta_3 + (\pi - \beta_3)$$

As a result, using Eq. 2, the tendon forces for closing action are obtained below:

$$\begin{aligned} F_1 = \Bigg\{ & u_1\left[\left(\frac{t_3}{2}\cos(\alpha_3-\theta_{123})-a_3\sin(\alpha_3-\theta_{123})\right)\left(\frac{t_2}{2}\cos(\alpha_2-\theta_{12})-a_2\sin(\alpha_2-\theta_{12})\right)\right] \\ & + u_2\left[\left(\frac{t_3}{2}\cos(\alpha_3-\theta_{123})-a_3\sin(\alpha_3-\theta_{123})\right)\left(a_2\sin(\alpha_2-\theta_{12})+L_1\sin(\alpha_2-\theta_1)-\frac{t_2}{2}\cos(\alpha_2-\theta_{12})\right)\right] \\ & + u_3\left[L_1\sin(\alpha_2-\theta_1)\left(a_3\sin(\alpha_3-\theta_{123})+L_2\sin(\alpha_3-\theta_{12})-\frac{t_3}{2}\cos(\alpha_3-\theta_{123})\right)+L_1\sin(\alpha_3-\theta_1)\left(\frac{t_2}{2}\cos(\alpha_2-\theta_{12})-a_2\sin(\alpha_2-\theta_{12})\right)\right]\Bigg\} \Bigg/ \\ & \left\{\left[\frac{t_3}{2}\cos(\alpha_3-\theta_{123})-a_3\sin(\alpha_3-\theta_{123})\right]\left[a_1\sin(\alpha_1-\theta_1)-\frac{t_1}{2}\cos(\alpha_1-\theta_1)\right]\left[\frac{t_2}{2}\cos(\alpha_2-\theta_{12})-a_2\sin(\alpha_2-\theta_{12})\right]\right\} \end{aligned}$$

$$F_2 = \left\{u_2\left[a_3\sin(\alpha_3-\theta_{123})-\frac{t_3}{2}\cos(\alpha_3-\theta_{123})\right]+u_3\left[\frac{t_3}{2}\cos(\alpha_3-\theta_{123})-a_3\sin(\alpha_3-\theta_{123})-L_2\sin(\alpha_3-\theta_{12})\right]\right\}\Big/$$
$$\left\{\left[a_2\sin(\alpha_2-\theta_{12})-\frac{t_2}{2}\cos(\alpha_2-\theta_{12})\right]\left[a_3\sin(\alpha_3-\theta_{123})-\frac{t_3}{2}\cos(\alpha_3-\theta_{123})\right]\right\}$$

$$F_3 = u_3\Big/\left[a_3\sin(\alpha_3-\theta_{123})-\frac{t_3}{2}\cos(\alpha_3-\theta_{123})\right]$$

If extension motion of the fingers are considered then, extension forces F_1', F_2', F_3' are obtained similarly.

$$x_1' = a_1\cos\theta_1+\frac{t_1}{2}\sin\theta_1$$
$$y_1' = a_1\sin\theta_1-\frac{t_1}{2}\cos\theta_1$$
$$x_2' = L_1\cos\theta_1+a_2\cos\theta_{12}+\frac{t_2}{2}\sin\theta_{12}$$
$$y_2' = L_1\sin\theta_1+a_2\sin\theta_{12}-\frac{t_2}{2}\cos\theta_{12}$$
$$x_3' = L_1\cos\theta_1+L_2\cos\theta_{12}+a_3\cos\theta_{123}+\frac{t_3}{2}\sin\theta_{123}$$
$$y_3' = L_1\sin\theta_1+L_2\sin\theta_{12}+a_3\sin\theta_{123}-\frac{t_3}{2}\cos\theta_{123}$$

Here x_i' and y_i' (i=1,2,3) denote position of the extensor tendon attachment points of the related phalanges.

$$F_{1x}' = F_1'\cos\alpha_1';\quad F_{2x}' = F_2'\cos\alpha_2';\quad F_{3x}' = F_3'\cos\alpha_3'$$
$$F_{1y}' = F_1'\sin\alpha_1';\quad F_{2y}' = F_2'\sin\alpha_2';\quad F_{3y}' = F_3'\sin\alpha_3'$$

α_i' (i = 1,2,3) are the angles of the extensor tendon forces with respect to the base frame and are given below.

$$\alpha_1' = \theta_1+(\pi+\beta_1)$$
$$\alpha_2' = \theta_1+\theta_2+(\pi+\beta_2)$$
$$\alpha_3' = \theta_1+\theta_2+\theta_3+(\pi+\beta_3)$$

As a result, using again Eq. 2, the tendon forces for opening action are obtained below:

$$F_1' = \left\{u_1\left[\left(a_3\sin(\alpha_3'-\theta_{123})+\frac{t_3}{2}\cos(\alpha_3'-\theta_{123})\right)\left(a_2\sin(\alpha_2'-\theta_{12})+\frac{t_2}{2}\cos(\alpha_2'-\theta_{12})\right)\right]\right.$$
$$-u_2\left[\left(a_3\sin(\alpha_3'-\theta_{123})+\frac{t_3}{2}\cos(\alpha_3'-\theta_{123})\right)\left(a_2\sin(\alpha_2'-\theta_{12})+L_1\sin(\alpha_2'-\theta_1)+\frac{t_2}{2}\cos(\alpha_2'-\theta_{12})\right)\right]$$
$$\left.+u_3\left[L_1\sin(\alpha_2'-\theta_1)\left(a_3\sin(\alpha_3'-\theta_{123})+L_2\sin(\alpha_3'-\theta_{12})+\frac{t_3}{2}\cos(\alpha_3'-\theta_{123})\right)-L_1\sin(\alpha_3'-\theta_1)\left(a_2\sin(\alpha_2'-\theta_{12})+\frac{t_2}{2}\cos(\alpha_2'-\theta_{12})\right)\right]\right\}\Big/$$
$$\left\{\left[a_3\sin(\alpha_3'-\theta_{123})+\frac{t_3}{2}\cos(\alpha_3'-\theta_{123})\right]\left[a_2\sin(\alpha_2'-\theta_{12})+\frac{t_2}{2}\cos(\alpha_2'-\theta_{12})\right]\left[a_1\sin(\alpha_1'-\theta_1)+\frac{t_1}{2}\cos(\alpha_1'-\theta_1)\right]\right\}$$

$$F_2' = \left\{ u_2 \left[a_3 \sin(\alpha_3' - \theta_{123}) + \frac{t_3}{2} \cos(\alpha_3' - \theta_{123}) \right] - u_3 \left[a_3 \sin(\alpha_3' - \theta_{123}) + L_2 \sin(\alpha_3' - \theta_{12}) + \frac{t_3}{2} \cos(\alpha_3' - \theta_{123}) \right] \right\} \Big/ \left\{ \left[a_3 \sin(\alpha_3' - \theta_{123}) + \frac{t_3}{2} \cos(\alpha_3' - \theta_{123}) \right] \left[a_2 \sin(\alpha_2' - \theta_{12}) + \frac{t_2}{2} \cos(\alpha_2' - \theta_{12}) \right] \right\}$$

$$F_3' = u_3 \Big/ \left[a_3 \sin\left(\alpha_3' - \theta_{123}\right) + \frac{t_3}{2} \cos\left(\alpha_3' - \theta_{123}\right) \right]$$

Appendix 3

Numerical parameters of the controller:

Γ_1=200	T_i=0.001
Γ_2=400	SF_e=3.3
Γ_3=600	$SF_{\dot{e}}$=0.5

References

1. Armstrong, T.J., Chaffin, D.B.: An investigation of the relationship between displacements of the finger and wrist joints and the extrinsic finger flexor tendons. J. Biomech. **11**, 119–128 (1978)
2. Landsmeer, J.M.F.: Study in the anatomy of articulation. Acta Morph. Neerlans Scand. **3**, 287–321 (1960)
3. Buchholz, B., Armstrong, T.J.: A kinematic model of the human hand to evaluate its prehensile capabilities. J. Biomech. **25**(2), 149–162 (1992)
4. Youm, Y., Gillespie, T.E., Flatt, A.E., Sprague, B.L.: Kinamatic investigation of normal MCP joint. J. Biomech. **11**, 109–118 (1978)
5. Buchner, H.J., Hines, M.J., Hemami, H.: A dynamic model for finger interphalangeal coordination. J. Biomech. **21**(6), 459–468 (1988)
6. An, K.N., Chao, E.Y., Cooney, W.P., Linscheid, R.L.: Normative model of human hand for biomechanical analysis. J. Biomech. **12**, 775–788 (1979)
7. Gregory, R.W.: Biomechanics and control of torque production during prehension. Thesis of Doctor of Philosophy, The Pennsylvania State University, (2002)
8. Jones, L.: Dextrous hands: Human, prosthetic and robotic: A survey. Presence: Teleoperators and Virtual Environments. **6**(1), 29–56 (1997)
9. Doshi, R., Yeh, C., LeBlanc, M.: The design and development of a gloveless endoskeletal prosthetic hand. J. Rehabil. Res. Dev. **35**(4), 388–395 (1998)
10. Bundhoo, V., Park, E.J.: Design of an artificial muscle actuated finger towards biomimetic prosthetic hands. 12th International Conference on Advanced Robotics ICAR, Seatle, USA, July pp. 18–20 (2005)
11. Morita, S., Shibata, K., Zheng, X.Z., Ito, K.: Prosthetic hand control based on torque estimation from EMG signals. Proceedings of the 2000 IEEE/RSJ International Conference on Intelligent Robots and Systems, Tokyo, Japan, Oct. 30–Nov. 5 pp. 389 –394 (2000)
12. Morita, S., Kondo, T., Ito, K.: Estimation of forearm movement from EMG signal and application to prosthetic hand control. Proceedings of the 2001 IEEE International Conference on Robotics & Automation, Seoul, South Korea, May 21–26, pp. 3692–3697, (2001)
13. Pollard, N., Gilbert, R.C.: Tendon arrangement and muscle force requirements for humanlike force capabilities in a robotic finger. Proceedings of the IEEE International Conference on Robotics and Automation (ICRA '02), Washington, USA, May 11–15, pp. 3755–3762 (2002)
14. Li, Z.M., Zatsiorsky, V.M., Latash, M.L.: The effect of extensor mechanism on finger flexor force. 24th Annual Meeting of the American Society of Biomechanics, University of Illinois at Chicago, USA, July 19–22 (2000)

15. Weghe, M.V., Rogers, M., Weissert, M., Matsuoka, Y.: The ACT hand: Design of the skeletal structure. Proceedings of the 2004 IEEE International Conference on Robotics, LA, USA, April 26–May 1, pp. 3375–3379 (2004)
16. Tsang, W., Singh, K., Fiume, E.: Helping hand: An anatomically accurate inverse dynamics solution for unconstrained hand motion. ACM SIGGRAPH /Eurographics Symposium of Computer Animation (SCA 2005), Los Angeles, California, USA, July 29–31, 319–328 (2005)
17. Fukaya, N., Toyama, S., Asfour, T., Dillmann, R.: Design of the TUAT/Karlsruhe humanoid hand. IEEE/RSJ International Conference on Intelligent Robots and Systems, Kagawa University, Takomotsu, Japan, 30 October–5 November, pp. 13–19 (2000)
18. Asfour, T., Berns, K., Dillmann, R.: The Humanoid Robot ARMAR. Proc. of the Second International Symposium on Humanoid Robots (HURO'99), Tokyo, Japan, October 8–9, pp. 174–180 (1999)
19. Jacobsen, S.C., Ko, H., Iversen, E.K., Davis, C.C.: Control strategies for tendon- driven manipulators. IEEE Control Syst. Mag. **10**(2), 23–28 (1990).
20. Yokoi, K., Tanie, K., Imamura, N., Kawai, T., Agou, K.: Design and control of a seven-degrees-of-freedom manipulator actuated by a coupled tendon-driven system. International Workshop on Intelligent Robots and Systems, Osaka, Japan, November 3–5, pp. 737–742 (1991)
21. Kawanishi, K., Hashizumi, H., Oki, Y., Nakano, Y., Fukuda, T., Vachkov, G., Arai, F., Hasegawa, Y.: Position and elasticity control for biomimetic robot finger. IEKON 2000 26th Annual Conference of the IEEE, Nagoya, Aichi, Japan, October 22–28, pp. 870–875 (2000)
22. Utkin, V.I.: Variable structure systems with sliding modes. IEEE Trans. Automat. Contr. **22**, 212–222 (1977)
23. Hung, J.Y., Gao, W., Hung, J.C.: Variable structure control: A Survey. IEEE Trans. Ind. Electron. **40**(1), 2–22 (1993)
24. Young, K.D., Utkin, V.I., Özgüner, Ü.: A control engineer's guide to sliding mode control. IEEE Trans. Control Syst. Technol. **7**(3), 328–342 (1999)
25. Herman, P.: Sliding mode control of manipulators using first-order equations of motion with diagonal mass matrix. J. Franklin Inst. **342**, 353–363 (2005)
26. Ertugrul, M., Kaynak, O., Sabanovic, A.: A comparison of various vss techniques on the control of automated guided vehicles. In: Proceedings of the IEEE International Symposium on Industrial Electronics, Athens, Greece, July 10–14, pp. 837–842 (1995)
27. Yagiz, N.: Alternative approaches in sliding mode control theory. In: Proceedings of the 2nd International Symposium on Mechanical Vibrations, September 25–28, Islamabad, Pakistan, pp. 94–103 (2000)
28. Palm, R.: Sliding mode fuzzy control. In: Proceedings of the IEEE International Conference on Fuzzy Systems, San Diego, CA, pp. 519–526 (1992)
29. Choi, S.B., Kim, J.: A fuzzy-sliding mode controller for robust tracking of robotic manipulators. Mechatronics **7**(2), 199–216 (1997)
30. Tzafestas, S.G., Rigatos, G.G.: A simple robust sliding-mode fuzzy-logic controller of the diagonal type. J. Intell. Robot. Syst. **26**, 353–388 (1999)
31. Kuo, C.L., Li, T.H.S., Guo, N.R.: Design of a novel fuzzy sliding-mode control for magnetic ball levitation system. J. Intell. Robot. Syst. **42**, 295–316 (2005)
32. Choi, S.B., Cheong, C.C., Park, D.W.: Moving switching surfaces for robust control of second-order variable structure systems. Int. J. Control **58**(1), 229–245 (1993)
33. Iliev, B., Kalaykov, I.: Improved sliding mode robot control—a fuzzy approach. In Proceedings of the Third International Workshop on Robot Motion and Control, November 9–11, pp. 393–398 (2002)
34. LaViola, J.J. Jr.: A survey of hand posture and gesture recognition techniques and technology. Technical Report CS-99–11, Department of Computer Science, Brown University, June (1999)
35. H. Gray, 1858, "Gray's Anatomy: Descriptive and Surgical", Great Britain, (http://en.wikipedia.org/wiki/Grays_Anatomy; last visited 25.05.2006)
36. Craig, J.J.: Introduction to Robotics: Mechanics and Control-Second Edition. Addison- Wesley, USA (1989)